Published in final edited form as:

Reprod Biol. 2016 March ; 16(1): 13–26. doi:10.1016/j.repbio.2015.12.004.

Slc20a2 deficiency results in fetal growth restriction and placental calcification associated with thickened basement membranes and novel CD13 and lamininα1 expressing cells

Mary C. Wallingford[a], **Hilary S. Gammill**[b], and **Cecilia M. Giachelli**[a,*]

Mary C. Wallingford: marycwallingford@gmail.com; Hilary S. Gammill: hgammill@uw.edu; Cecilia M. Giachelli: ceci@uw.edu

[a]University of Washington, Department of Bioengineering, 3720 15th Ave NE, Seattle, WA 98195, USA

[b]University of Washington, Department of Obstetrics and Gynecology, Seattle, WA 98195, USA

Abstract

The essential nutrient phosphorus must be taken up by the mammalian embryo during gestation. The mechanism(s) and key proteins responsible for maternal to fetal phosphate transport have not been identified. Established parameters for placental phosphate transport match those of the type III phosphate transporters, Slc20a1 and Slc20a2. Both members are expressed in human placenta, and their altered expression is linked to preeclampsia. In this study, we tested the hypothesis that Slc20a2 is required for placental function. Indeed, complete deficiency of Slc20a2 in either the maternal or embryonic placental compartment results in fetal growth restriction. We found that Slc20a2 null mice can reproduce, but are subviable; ~50% are lost prior to weaning age. We also observed that 23% of Slc20a2 deficient females develop pregnancy complications at full term, with tremors and placental abnormalities including abnormal vascular structure, increased basement membrane deposition, abundant calcification, and accumulation of novel CD13 and lamininα1 positive cells. Together these data support that Slc20a2 deficiency impacts both maternal and neonatal health, and Slc20a2 is required for normal placental function. In humans, decreased levels of placental Slc20a1 and Slc20a2 have been correlated with early onset preeclampsia, a disorder that can manifest from placental dysfunction. In addition, preterm placental calcification has been associated with poor pregnancy outcomes. We surveyed placental calcification in human preeclamptic placenta samples, and detected basement membrane-associated placental calcification as well as a comparable lamininα1 positive cell type, indicating that similar mechanisms may underlie both human and mouse placental calcification.

Keywords

Laminin; Placental calcification; Phosphate transport; *PiT-2*; *Slc20a2*

[*]*Corresponding author*. Tel.: +1 206 543 0205; fax: +1 206 616 9763. http://dx.doi.org/10.1016/j.repbio.2015.12.004.

Conflict of interest

None declared.

1. Introduction

All living organisms require phosphorus. It is a key component of cell membranes and DNA, and plays important roles in energetics and protein signaling. Phosphorus is found circulating through blood vessels and traveling between extracellular and intracellular environments in the form of phosphoric acid, $H_2PO_4^-$. The majority of phosphorus is found in bone in the form of hydroxyapatite crystals, $Ca_{10}(PO_4)_6(OH)_2$.

Intracellular concentrations of phosphorus greatly exceed extracellular concentrations observed in serum, and phosphorus must move against a concentration gradient to produce high intracellular concentrations [1]. Transmembrane transporters move phosphorus across the cell membrane in the form of phosphoric acid. In medical literature, the term phosphate (technically referring to PO_4^{-3}) is often used when referring to either elemental phosphorus or phosphoric acid. Thus, proteins that transport phosphoric acid are referred to as phosphate transporters, including the type III sodium-dependent phosphate transporters Slc20a1/PiT-1 and Slc20a2/PiT-2.

Phosphorus is consumed through diet in adults and is transferred from the mother to the fetus during pregnancy. The human fetus contains ~16–30 g of phosphorus at birth, with the majority obtained at the time of bone growth during late gestation [2,3]. Despite the rapid cell division, extensive protein signaling, bone development, and other phosphate-dependent processes that occur during this time in development, maternal to fetal phosphate transport mechanisms remain unknown. Several characteristics have been established, however. Fetal serum has been shown to have a higher concentration of phosphate than maternal serum; because transport flux is against a concentration gradient, transfer is believed to be active [4,5]. In addition, placental phosphate transport is regulated by parathyroid hormone, pH, and sodium availability, characteristics that match those of Slc20a1 and Slc20a2 [6–8].

The majority of maternal to fetal nutrient transfer occurs across the placenta. Recent studies support that Slc20a1 and Slc20a2 are poised to control placental phosphate transport. Both Slc20a1 and Slc20a2 are expressed in human placentas, and their altered expression is associated with placental dysfunction and preeclampsia [9,10]. Slc20a1 global KO mice are early embryonic lethal, precluding analysis of Slc20a1 roles in the late term placenta [11–13]. In this study, we sought to test the hypothesis that Slc20a2 plays an important role in placental function.

2. Materials and methods

2.1. Specimens

2.1.1. Mouse specimens—All mouse work was performed with IACUC approval (protocol #2224-08) from the University of Washington, Seattle. C57BL/6NTac-Slc20a2<tm1a(EUCOMM)Wtsi>/Ieg (Slc20a2+/−) mice were purchased from the European Mouse Mutant Archive (EMMA). Wildtype (Slc20a2+/+) C57Bl/6 mice were purchased from Jackson labs (Sacramento, CA) and from Taconic labs (Hudson, NY). At least 3 animals/genotype were analyzed for each experiment; specific animal numbers are noted throughout.

2.1.2. Human specimens—Placentas were collected with IRB approval from the University of Washington, Seattle; all subjects provided written informed consent for placental collection. Preeclampsia was defined by standard clinical criteria [14]. Gestational ages were between 33 and 40 weeks, specifically: 33 weeks 2 days, 35 weeks and 0 days, and 39 weeks 1 day.

2.2. Western blotting

Kidney and placental lysates were collected and treated with a protease inhibitor cocktail (Roche). Lysates were denatured at 90 °C in Laemli Buffer containing β-Mercaptoethanol, and run in a 10% SDS Page gel. 40 μg of protein was loaded per well. Proteins were then transferred to a PVDF membrane, and blots were blocked with 5% milk. Slc20a2 antibody (provided by Dr. Moshe Levi, UC) was used at a concentration of 3.2 μg/mL and the primary antibody was detected with Peroxidase-conjugated AffiniPure Goat Anti-Rabbit IgG (H+L) (Jackson ImmunoResearch, 111-035-144) at 3 μg/mL. Western Lighting Plus ECL (PerkinElmer), was used to detect HRP signal. In order to determine loading control values, the western blot was stripped with Restore Plus Western Blot Stripping Buffer (Thermo Scientific PI-46430) and reprobed with β-actin (Abcam ab8227). Densitometry was performed with ImageJ.

2.3. RNA extraction, cDNA synthesis, and qPCR

Placenta tissue RNA was extracted using the RNeasy Mini Kit according to the manufacturer's directions (Qiagen, 74106). cDNA was made with 1000ug of total RNA per sample using the Omniscript Reverse Transcriptase kit (Qiagen, 205113). TaqMan probes conjugated with a fluorochrome reporter (FAM) tag at the 5′-end and an MGB quencher at the 3′-end were used to assess expression levels. Amplification and detection were carried out in 96-well optical plates on an ABI Prism 7000 Sequence Detection System (Applied Biosystems), with TaqMan Universal PCR 2X master mix (Life Technologies, 4305719) in a final volume of 20 μL per reaction. Each reaction was carried out at 50 °C for 2 min, 95 °C for 10 min, followed by 40 cycles of 95 °C for 15 s, and 60 °C for 1 min. Results were analyzed with the manufacturer's software, SDS 1.1 (Applied Biosystems). Gene mRNA expression was normalized to the housekeeping gene 18S (Life Technologies, Cat. No. 4308329) using the quantitative method ($2^{-\Delta\Delta C_T}$, where $\Delta\Delta C_T = [C_T^{\text{gene}} - C_T^{18S}]_{\text{treated}} - [C_T^{\text{gene}} - C_T^{18S}]_{\text{control}}$). The following Life Technologies Taqman Assays were used: Slc20a2 (Mm00660204_mH), IL-6 (Mm00446190_m1), Il-10 (Mm00439614_m1), Arg1 (Mm00475988_m1), TNF (Mm00443258_m1).

2.4. Histology

2.4.1. Fixation, embedding and sectioning—Samples were dissected and fixed in 4% paraformaldehyde (PFA)/PBS overnight at 4 °C. After whole mount images were taken, the tissue was dehydrated in 100% EtOH, treated with Xylenes and embedded in paraffin wax at 60 °C. Sections were cut at 7 μm on a Leica RM2135 microtome, dried, and baked at 60 °C for 1 h prior to further processing.

2.4.2. Immunostaining—Immunofluorescence was performed as previously published [15], but treated with a serum block as opposed to a milk block. Heat mediated antigen

retrieval was performed with 0.01 M Tris Base pH10.0. The following antibodies and antibody concentrations were used:

Slc20a2 (gift of Dr. M. Levi, University of Colorado, 8 μg/mL)

Slc20a2 (Santa Cruz, sc-377326, 10 μg/mL)

Cytokeratin 7 (Abcam, ab181598, 10 μg/mL)

Tpbpα (Abcam, ab104401, 10 μg/mL)

SM22α (Abcam, ab10135, 20 μg/mL)

CD13 (R&D Systems, AF2335, 5 μg/mL)

Lamα1 (Sigma–Aldrich, L9393, 5 μg/mL)

Ki67 (Abcam, ab66155, 5 μg/mL)

OPN (R&D Systems, AF808, 2 μg/mL)

vWF (Dako, A0082, 15.5 μg/mL)

CD86 (eBioscience, 14-0861, 5 μg/mL)

Secondary antibodies included: DyLight 488-Conjugated AffiniPure Donkey Anti-Goat IgG (Jackson ImmunoResearch, 705-485-147, 7.5 μg/mL), DyLight 549-Conjugated AffiniPure Donkey Anti-Rabbit IgG (Jackson ImmunoResearch, 711-505-152, 7.5 μg/mL), Peroxidase-conjugated AffiniPure Goat Anti-Rabbit IgG (H+L) (Jackson ImmunoResearch, 111-035-144, 3 μg/mL), Alexa Fluor 488-Conjugated AffiniPure Donkey Anti-Rabbit IgG (Jackson ImmunoResearch, 711-545-152, 15 μg/mL), Alexa Fluor 488-conjugated AffiniPure Donkey Anti-Mouse (Jackson ImmunoResearch, 715-545-151, 7.5 μg/mL), DyLight 549-conjugated AffiniPure Donkey Anti-Rabbit IgG (H+L) (Jackson ImmunoResearch, 711-505-152, 7.5 μg/mL).

2.4.3. Alizarin red—Alizarin Red was performed as in Speer et al. (2009) with the exception of a 1 h 15 min Alizarin Red treatment time [1].

2.4.4. PAS—Periodic Acid Schiff (PAS) staining was performed with Periodic Acid (Sigma, P7875, 5 min), Schiff's Reagent (Sigma, 3952016, 20 min) and Harris Hematoxylin counterstain (Sigma, HHS32, 1 min).

2.4.5. Hematoxylin and eosin—Hematoxylin and Eosin staining was performed as previously published [16]. Specific stains used included Harris Hematoxylin (Sigma HHS32) and Eosin Y (Sigma E4382).

2.5. Imaging

Digital images of fixed whole embryos were captured on a Nikon SMZ-1500 stereomicroscope equipped with a Nikon D5100 DSLR camera. Digital images of sectioned embryos were taken with a Nikon Eclipse E800 inverted fluorescence microscope and an RS Photometrics Coolsnap color digital camera with Metamorph Version 6.3r7 or Nikon Elements and converted with Irfanview Version 4.2.3, except for the images in Figs. 2 and 3.

2.6. Quantification of placental features

2.6.1. Placental width—PAS stained sections were used to determine placental width of Slc20a2+/+ and Slc20a2+/− placentas using Image-J Version 1.46r (http://imagej.nih.gov/ij). The student's t-test was used to test the null hypothesis that there were no differences between genotypes.

2.6.2. Placental calcification—Alizarin Red stained sections were used to determine the degree of calcification in Slc20a2+/+and Slc20a2+/− placentas. Placentas were scored blindly by a lab member who had no previous experience with the specimens. Placentas were scored visually by the portion of tissue covered with Alizarin Red positive staining as follows: 0 = ~0%, 1 = ~1–20%, 2 = ~21–40%, 3 = ~41–60%, 4 = ~61–90%, 5 = ~91–100%. The student's *t*-test was used to test the null hypothesis that there were no differences between genotypes.

3. Results

3.1. Slc20a2 displays distinct localization patterns in the placenta

Slc20a2 expression at E9.5, E12.5, and E15.5 was assessed by western blotting with placenta lysates normalized to β-actin (Fig. 1A and B) and by qPCR with placenta mRNA normalized to 18S (Fig. 1C). Slc20a2 mRNA markedly increased during gestation. A significant difference in Slc20a2 mRNA level was detectable in heterozygous mice at E12.5 and E15.5; E15.5 Slc20a2−/− placentas were used as a negative control (Fig. 1C).

Slc20a2 protein localization in mouse placenta sections was determined by immunofluorescence. We tested co-localization of Slc20a2 and the trophoblast markers cytokeratin 7 (CK7) or trophoblast specific protein alpha (Tpbpα) at E9.5, E10.5 and E15.5. At E9.5, trophoblast cells in the placenta proper did not express Slc20a2 (Fig. 2A and E and data not shown). At E10.5, Slc20a2 only co-localized with CK7 positive cells that were in close proximity to the chorioallantoic plate that contained large nuclei (Fig. 2B and F). Slc20a2 displayed a striking intracellular localization pattern in these cells that was detected with two different anti-Slc20a2 antibodies and indicative of vesicular organelles (Supplemental Fig. 1). Slc20a2 expression was maintained in CK7 positive cells near the chorioallantoic plate at E15.5 (Fig. 2C and G). Slc20a2 did not co-localize with the spongiotrophoblast marker Tpbpα at E9.5, E10.5 or E15.5 (Fig. 2D and H and data not shown). Slc20a2 positive that were negative for CK7 and Tpbpα were distributed throughout the placental labyrinth, the site of exchange between the fetal and maternal blood supply [17].

Supplementary Fig. 1 related to this article can be found, in the online version, at doi: 10.1016/j.repbio.2015.12.004.

In order to determine whether Slc20a2 is expressed in vascular cells in the E15.5 decidua, we stained consecutive sections with Slc20a2 and several markers as follows: von Willebrand factor (vWF) was used to identify endothelial cells, smooth muscle 22 alpha (SM22α) was used to identify smooth muscle cells, and aminopeptidase N (CD13) was used to identify pericytes. We found that Slc20a2 did not localize to endothelial cells or smooth

muscle cells in the E15.5 decidua (Fig. 3A–D). Slc20a2 did localize to pericytes on the vessel periphery (Fig. 3E and F). The Slc20a2 staining pattern in the labyrinth was further confirmed to be in pericytes with alpha smooth muscle actin co-localization and anatomical localization (data not shown).

3.2. Slc20a2 deficient mice are subviable

In order to test the hypothesis that Slc20a2 is required for normal placental function, we obtained *Slc20a2* KO-first mice containing one KO-first allele from the European Mouse Mutant Archive (EMMA). Heterozygous and homozygous KO intercrosses revealed preweaning subviability (Tables 1 and 2). In addition, Slc20a2 deficient females were found to be poor breeders. First-time Slc20a2+/−mothers yielded no neonates that survived to weaning age, where as control first-time Slc20a2+/+ mothers bred successfully. First-time Slc20a2+/− mothers in a trio-breeding situation with minimal cage disturbances generated pups, but 31% never yielded pups (N = 13 female breeders).

In order to assess preweaning viability, we examined the frequency and number of Slc20a2+/+, +/− and −/− mice generated by heterozygous intercrosses. A heterozygous intercross should generate 25%+/+, 50%+/− and 25%−/− animals. A total of 42+/+ mice were weaned from 17 heterozygous intercrosses. Using this value, we would expect to generate 84+/− mice and 42−/− mice, and to observe an average litter size of 9.3. However, we observed only 5.9 mice on average per litter at weaning. Genotyping determined that only 55 Slc20a2+/− mice and 16 Slc20a2−/− mice were present at weaning, indicating a 28% loss of Slc20a2+/− mice and a 57% loss of Slc20a2−/− mice prior to weaning (Table 1, N = 17 litters). Similarly, small litters were generated from homozygous null intercrosses; on average 5.5 mice were present at weaning, indicating a 55% loss of Slc20a2−/− mice prior to weaning (Table 2, N = 6 litters). We then assessed whether complete Slc20a2 deficiency manifests in fetal growth restriction by measuring embryonic weights at E17.5. Slc20a2+/− placentas with heterozygous embryonic and maternal placental compartments were used as controls and compared to embryos and placentas that completely lacked Slc20a2 in either the embryonic or maternal placental compartments. Reabsorbing embryos were observed and were excluded from the analysis. We found that loss of Slc20a2 from either the embryonic (p-value = 0.0004) or maternal (p-value = 0.003) compartment leads to a significant decrease in embryonic weight at E17.5; n = 4–5; N = 14 (Fig. 4A). In contrast, complete loss of Slc20a2 from either the embryonic (p-value = 0.2) or maternal (p-value = 0.09) placental compartment does not change placental weight significantly at E17.5; n = 4–5; N = 13 (Fig. 4B). The embryo/placenta ratio is unchanged with embryonic loss of Slc20a2 (p-value = 0.29). However, complete loss from the maternal compartment leads to a significant increase in the embryo/placenta ratio at E17.5 (p-value = 0.02); n = 4–5; N = 13 (Fig. 4C).

Finally, we found that 23% of pregnant Slc20a2+/− females displayed full term pregnancy-associated morbidity (N = 13). Preliminary results revealed high albumin:creatinine ratio in morbid Slc20a2 deficient females (ACR) (WT = 3.7 ACR and Het = 10.7 ACR). Serum phosphorus was also increased (WT = 10.4 mg/dL; Het = 13.2 mg/dL). However, serum calcium was within the normal range (WT = 10 mg/dL; Het = 8.8 mg/dL). We suspected that

the declining maternal health may be due to placental dysfunction and performed histological analysis of placental tissue.

3.3. Slc20a2 deficiency can result in increased placental calcification

Placentas from affected Slc20a2+/− females appeared thin and abnormal in color at the time of dissection. E18.5 Embryos from a Slc20a2+/− intercross were genotyped to determine placentas with Slc20a2+/+, +/− or −/− fetal compartments. Sites of discoloration were observed in all placentas from +/− females, and those with a −/− embryonic placental compartment were observed to have abnormal vasculature (representative examples in Fig. 5A–D). Placental height was reduced compared to placentas from Slc20a2+/+ controls, irrespective of embryonic genotype ($n = 3$ per genotype) (Fig. 5E).

Disrupted phosphorus handling has been associated with vascular calcification in several diseases and disease models. For example, humans and mice with mutations in Slc20a2 or XPR1 develop Idiopathic Basal Ganglia Calcification, a disease characterized by calcification of cerebral blood vessels [18,19]. Thus, Slc20a2 has been hypothesized to play an anti-calcific role in the vasculature. The placenta is a highly specialized and regenerative component of the circulatory system that contains an abundance of specialized vascular structures across which exchange between maternal and fetal circulation occurs [17]. We hypothesized that reduced transport across the placenta in Slc20a2 deficient mice leads to a phosphate build-up in the placenta, and calcification of placental vasculature. We determined whether Slc20a2+/− placentas in the labyrinth (Fig. 5F), the decidua (Fig. 5G–I and D), and the chorioallantoic plate (shown in Fig. 7). >Staining of consecutive sections with Alizarin Red, H&E, or Periodic Acid Schiff's (PAS) was used to assess the overall structure of the placenta and decidua. Placental structure was striking; the decidua was compact, vessels were missing and abnormal in structure, and the junctional layer was not identifiable (Fig. 6). Vessels in the decidua were further examined with vWF and laminin antibodies that identified increased laminin deposition or retention in the vessels walls, but no difference in vWF on the vessel intima (Supplemental Fig. 2).

Supplementary Fig. 2 related to this article can be found, in the online version, at doi: 10.1016/j.repbio.2015.12.004.

3.4. Placental calcification is adjacent to sites of increased basement membrane deposition

We then tested whether placentas from Slc20a2+/+ and Slc20a2+/− females develop distinct placental calcification patterns by staining with Alizarin Red. Calcification observed in Slc20a2+/+ placentas was minimal (Fig. 7A) and matched published results for wildtype (WT) mice [20]. In contrast, Slc20a2+/− placentas consistently displayed more calcification than Slc20a2+/+ controls (Fig. 7B). Placental sections were scored blindly for calcification level as described in Section 2.6.2, and revealed a clear increase in calcification level in the Slc20a2+/− placentas compared to healthy controls (Supplemental Fig. 3). PAS staining and H&E were used to assess the labyrinth structure of Slc20a2+/+ and Slc20a2+/− placentas. PAS revealed a compact decidua, as well as a basement membrane-laden labyrinth with

abnormal structure in Slc20a2+/− placentas (Fig. 7C–F). H&E staining further confirms abnormal labyrinth structure and highlights the calcified lesions (Fig. 7G–H).

Supplementary Fig. 3 related to this article can be found, in the online version, at doi: 10.1016/j.repbio.2015.12.004.

Close examination of Alizarin Red staining revealed that the mineral was commonly found adjacent to basement membrane. In order to determine if this is the case, consecutive placenta sections were stained with Alizarin Red and PAS. Indeed, Alizarin Red positive sites were found lining enlarged basement membranes. In rare cases, basement membrane at the chorioallantoic plate had ruptured and the exposed spaces contained Alizarin Red positive mineral (Fig. 7I–L).

3.5. Lamininα1 is associated with abnormal basement membranes and calcified tissue

Laminin chains are an essential component of basement membranes [21,22], and Lamininα1 (Lamα1) is expressed very early in development in primitive endoderm cells that line the inner periphery of the blastocyst inner cell mass [23]. Lamα1 has also been shown to act as a scaffold for calcification in cell free systems [24,25]. We determined localization of Lamα1 in +/+ and +/− placentas. In Slc20a2+/+ placentas, Lamα1 localized to the Reichert's Membrane and thin basement membranes throughout the labyrinth (Fig. 8A). Lamα1 displayed a similar localization pattern in Slc20a2+/− placentas; however, the Reichert's Membrane of the chorioallantoic plate and the labyrinth zone had more prominent Lamα1 staining compared to Slc20a2+/+ placentas (Fig. 8B). The Lamα1 staining pattern highlighted abnormal vascular structure in the labyrinth of Slc20a2+/− placentas (Fig. 8D and E). Examination of regions of the labyrinth that contained minimal calcification suggested that mineral lined the basement membranes (Fig. 8F). Similarly, basement membranes in the chorioallantoic plate were Lamα1 positive, thickened, and frequently lined by mineral (Fig. 8G–I). Lastly, we observed an abundance of small round Lamα1 positive cells within the calcified tissue that was adjacent to chorioallantoic basement membranes (Figs. 8H and 9A).

3.6. Slc20a2 deficiency and placental calcification are characterized by the presence of a novel CD13 and Lamα1 positive cell type

A population of round cells was observed at the calcification site in Slc20a2+/− placentas, some of which were Lamα1 positive (Fig. 9A). In order to characterize this cell type, we performed immunohistochemistry of known markers. The cells that clustered at the calcified sites were uniformly positive for CD13, a marker of several cell types including: pericytes/perivascular cells that support vasculature and play a role in blood brain barrier permeability [26], mesenchymal stem cells proposed to regulate immunomodulating peptides as well as vasoactive and neuropeptide hormones [27], and pro-inflammatory monocytes mediating adhesion and phagocytosis [28,29] (Fig. 9B). A small number of the cells were also Slc20a1 positive (arrowhead in Fig. 9B). Morphologically similar CD13 positive cells were sparse in WT placenta. The small number of round CD13 positive cells localized only to the labyrinth, and were not detected next to the chorioallantoic basement membrane. In addition, all of the round CD13 positive cells detected in the WT mouse placenta uniformly co-expressed

Slc20a1 (arrows in Fig. 9C). We also found that these cells are Ki67 positive in WT tissue (arrows in Fig. 9D).

In order to determine whether the CD13 positive cells are a mature monocyte population, we stained for the costimulatory molecule CD86, a pan monocyte marker with highest expression in M1 populations [30,31]. We found that the CD13 positive cells in the labyrinth of both Slc20a2+/+ and Slc20a2 +/− placentas were CD86 positive, confirming the presence of CD13 positive monocytes in the placentas (Fig. 9E–H). However, the CD13 positive cells clustered at the calcified site adjacent to the chorioallantoic plate basement membrane were CD86 negative (data not shown), supporting that they are not M1-type macrophage/monocyte cells. To determine whether macrophage infiltration may be increased in Slc20a2-deficient conditions, we examined the expression level of the macrophage markers TNFα (M1) and Arg1 (M2) in Slc20a2+/+ and Slc20a2+/− E15.5 placenta, $p = 0.015$ and $p = 0.020$, respectively. TNFα and Arg1 qPCR supported that there may be increased macrophage infiltration, but did not identify altered macrophage polarization, $p = 0.827$ (Supplemental Fig. 4). In contrast, complete loss of Slc20a2 results in significantly reduced levels of both TNFα and Arg1 mRNA, $p = 0.006$ and $p = 0.011$, respectively (Supplemental Fig. 4).

Supplementary Fig. 4 related to this article can be found, in the online version, at doi: 10.1016/j.repbio.2015.12.004.

Next, we evaluated whether the CD13 positive cells at the calcified site were indeed the laminin α1 positive cells that we observed. Co-staining for CD13 and Lamα1 revealed two distinct populations at the calcified site (Fig. 9I–P). We found that the morphologically uniform CD13 positive population at the calcified site contained both Lamα1 positive cells (arrows in Fig. 9M–P) and Lamα1 negative cells (asterisk in Fig. 9I and K). In summary, the calcified +/− placentas contained at least three distinct CD13 positive cell populations that are morphologically similar but are characterized by distinct markers, including CD13 positive/CD86 positive/Lamα1 negative cells, CD13 positive/CD86 negative/Lamα1 positive cells and CD13 positive/CD86 negative/Lamα1 negative cells.

3.7. Preeclamptic human placentas contain placental calcification and laminin α1 positive cells

Placental calcification has been associated with poor pregnancy outcomes [32–34]. In order to determine whether calcification was present in preeclampsia placentas, we obtained anterior and posterior ($n = 3$) human placental specimens. Indeed, both anterior (Fig. 10A and B) and posterior tissue (Fig. 10C and D) stained positively for calcification by Alizarin Red. In some cases, the calcified lesions surrounded basement membrane-containing nodules (asterisk in Fig. 10B), similar to sites identified in mouse tissue (asterisk in Fig. 5I). Examination of the more weakly calcified human chorionic villi (analogous to the mouse labyrinth in function) showed an association of calcification with basement membranes (arrows in Fig. 10D). In addition, round Lamα1 positive cells reminiscent of those identified in the mouse were observed at Lamα1 positive basement membranes adjacent to sites of calcification (Fig. 10 E–L, arrows in I–L). Low magnification views of laminin and CD13 co-staining are available in Supplemental Fig. 5.

Supplementary Fig. 5 related to this article can be found, in the online version, at doi: 10.1016/j.repbio.2015.12.004.

4. Discussion

We found that Slc20a2−/− neonates can be born, but are subviable. In addition, complete deficiency of Slc20a2 in either the maternal or embryonic placental compartments resulted in fetal growth restriction. Slc20a2 deficient females were poor breeders, and 23% developed full term morbidity associated with abnormal placental vascular morphology and abundant placental calcification. Together these data support that Slc20a2 is required for normal placental function, and that Slc20a2 deficiency impacts both maternal and neonatal health.

As has been shown in human, we found that Slc20a2 was poised to regulate maternal-fetal phosphate transport in the mouse. Slc20a2 localized to pericytes and CK7 positive giant cells in the mature E15.5 placenta. Loss of the primary placental phosphate transporter would likely result in retention of phosphate in the placenta, as well as a deficit of phosphate in the developing embryo. Indeed, our finding of abundant mineral deposition in the placenta supports that this may be the case in Slc20a2 deficient mice. Increased mineralization may also explain the increased embryo/placenta weight ratio we observed when Slc20a2+/− embryos were generated by Slc20a2−/− females. Evaluation of embryonic phosphorus and hydroxyapatite levels will be required to determine whether there is a functional loss of Pi transport and Pi-dependent processes in the embryo. Of note, a complete lack of maternal to fetal phosphate transport would be expected to result in fully penetrant embryonic lethality. It is likely that Slc20a1 and passive diffusion both partially compensated for Slc20a2 loss during gestation. In support of this idea, Slc20a1 loss has previously been shown to result in a compensatory increase in expression of Slc20a2 [35]. When compared to embryos supported by placentas of Slc20a2+/− maternal and fetal genotypes, complete loss of Slc20a2 in either the maternal or fetal placental compartments resulted in fetal growth restriction. This result supports that Slc20a2 is required in both the maternal and fetal placental compartments. Furthermore, these data suggest that placental phosphate transport may involve a two-step transport mechanism, for example (1) transport out of the maternal circulation and (2) transport into the fetal circulation, or there may be unidentified phosphate transport-independent roles of Slc20a2, as is the case for Slc20a1 [36].

Human placentas have been reported to develop calcification, and placental calcification has been associated with pregnancy complications, such as viral infection [32–34]. Despite this, placental calcification pathology and impact on maternal health are poorly understood. As the first placental calcification mouse model, the Slc20a2 deficient mouse will be a useful tool for developing mechanistic hypotheses and testing candidate preventative treatments. Of note, reduced Slc20a2 expression has been linked to cases of preeclampsia, in which premature delivery was required; these pregnancies demonstrated decreased placental Slc20a1 and Slc20a2 expression in both the fetal and maternal placental compartments, compared to normotensive controls from premature deliveries [10]. Furthermore, other phenotypes we observe in Slc20a2 deficient mice have been linked to preeclampsia and hypertension during pregnancy, including basement membrane thickening [37–39]. A

literature search also revealed several preeclampsia cases in which factors that we identify as pro-calcific or anti-calcific molecules were altered in pre-eclampsia versus normotensive cases, including endosomal alkaline phosphatase [40], osteoprotegrin [41] and calcitonin [42,43]. Unfortunately, placental calcification was not examined in any of these studies. Future work will determine whether circulating levels of calcific factors do indeed correlate with placental calcification, and whether placental calcification levels correlate with blood pressure and other end-organ manifestations of preeclampsia. Should this be the case, circulating calcific factors may provide novel early warning diagnostic biomarkers and lead to identification of novel therapeutic targets for preeclampsia.

Physically, it remains unknown how exactly Slc20a1 or Slc20a2 transport phosphate into cells. Endocytic processes may play a role, as global loss of Slc20a1 disrupts yolk sac endocytosis [8]. Slc20a2 localized to intracellular puncta is indicative of endosomes. The protein localization provides clues for spatial understanding of how Slc20a1 and Slc20a2 may transport phosphate into the cell. Finally, both phosphate transporters also act as viral transporters, a process that can involve dynamic membrane fusion events. Probing of control and mutant Slc20a2 constructs by biochemical inhibition and X-ray crystallography is needed to elucidate the specific biophysical transport mechanism(s).

This work identified three distinct CD13 positive populations of round cells that are morphologically similar but characterized by specific combinations of markers, including CD13 positive/CD86 positive/Lamα1 negative cells, CD13 positive/CD86 negative/Lamα1 positive cells and CD13 positive/CD86 negative/Lamα1 negative cells. The CD13 positive/CD86 positive/Lamα1 negative cells were found in Slc20a2+/+ and +/− labyrinth tissue, and the CD13 positive/CD86 negative/Lamα1 positive cells, and CD13 positive/CD86 negative/Lamα1 negative cells were found specifically at the calcification sites in Slc20a2+/− chorioallantoic plates. CD13 can marks pericytes, mesenchymal stem cells, and monocytes. The gross morphology of these cells indicates that they are not pericytes. The expression of CD86 confirms that the round labyrinth CD13 positive cells have an M1 identity. However, the lack of CD86 in the round CD13 positive cells clustered at the calcified sites indicates that these are not M1 cells. In conclusion, this novel population may be an undifferentiated myeloid cell, a mesenchymal stem cell, or an alternate cell type that is not yet known to express CD13, such as a migratory fetal endothelial cell or trophoblast stem cell. It remains to be seen whether this population plays a role in the calcification, and if so whether it is playing an active role in mineral deposition or responding to it.

Currently, it is unclear whether placental calcification arises directly from Slc20a2 loss, follows Slc20a2-deficiency mediated placental damage, or both. We observed that vascular morphology is altered in calcified Slc20a2 deficient placentas, and this is accompanied by abnormal Lamα1 deposition. In mouse models, altered expression of various laminin chains has been linked to developmental vascular defects [21,22,44–47], and clinical studies suggest a role for laminin receptors and autoantibodies in preeclampsia [48–50]. Determination of whether altered Lamα1 deposition precedes or follows the vascular phenotype in Slc20a2 placentas and quantification of both expression and secretion of Lamα1 in the presence and absence of Slc20a2 will elucidate this etiology. Of note, molecular mechanisms controlling laminin secretion are largely unknown, and may involve

exocytosis [51–53]. Lastly, this work supports a protective and anti-calcific role for Slc20a2 in the placenta. The nucleation site and initial biochemical steps that promote mineralization in the placenta are not yet understood. Interestingly, Lamα1 can act as a scaffold for hydroxyapatite mineral deposition [24,25]. It is possible that Lamα1 protein on accessible placental basement membrane surfaces plays a central role in nucleation of placental calcification. In this case, protective mechanisms that increase deposition of basement membrane would result in a positive feedback loop of calcification and membrane deposition, eventually leading to the placental dysfunction, poor maternal health, and fetal growth restriction that we observed. Future work will investigate this model, and determine the relationship between placental calcification and placental dysfunction in humans.

Supplementary Material

Refer to Web version on PubMed Central for supplementary material.

Acknowledgments

We thank Nicholas W. Chavkin for blinded quantification of placental calcification, and Dr. Moshe Levi (UC) for sharing the rabbit anti-Slc20a2 antibody with us.

Sources of funding

The Giachelli Lab is funded by NIH grants HL62329, HL081785, and HL114611, and a grant from the DOD PRORP #OR120074. Dr. Wallingford is supported by the NIH NHLBI Training Grant: T32HL007828. The content of this project is solely the responsibility of the authors and does not necessarily represent the official views of the National Heart, Lung, and Blood Institute or the National Institutes of Health.

References

1. Virkki LV, Biber J, Murer H, Forster IC. Phosphate transporters: a tale of two solute carrier families. Am J Physiol Renal Physiol. 2007; 293:F643–54. [PubMed: 17581921]
2. Husain SM, Mughal MZ. Mineral transport across the placenta. Arch Dis Child. 1992; 67:874–8. [PubMed: 1519992]
3. Stulc J. Placental transfer of inorganic ions and water. Physiol Rev. 1997; 77:805–36. [PubMed: 9234966]
4. Schauberger C, Pitkin R. Maternal-perinatal calcium relationships. Obstet Gynecol. 1979; 53:7406.
5. Brunette M, Letendre S, Allard S. Phosphate transport through placenta brush border membrane. Adv Exp Med Biol. 1986; 208:543–8. [PubMed: 3565161]
6. Brunette MG, Auger D, Lafond J. Effect of parathyroid hormone on PO4 transport through the human placenta microvilli. Pediatr Res. 1989; 25:15–8. [PubMed: 2537487]
7. Brunette MG, Leclerc M, Ramachandran C, Lafond J, Lajeunesse D. Influence of insulin on phosphate uptake by brush border membranes from human placenta. Mol Cell Endocrinol. 1989; 63:57–65. [PubMed: 2546843]
8. Lajeunesse D, Brunette MG. Sodium gradient-dependent phosphate transport in placental brush border membrane vesicles. Placenta. 1988; 9:117–28. [PubMed: 3399488]
9. Nishimura M, Aito SN. Tissue-specific mRNA expression profiles of human solute carrier transporter superfamilies. Drug Metab Pharmacokinet. 2008; 23:22–44. [PubMed: 18305372]
10. Yang H, Kim T-H, Lee G-S, Hong E-J, Jeung E-B. Comparing the expression patterns of placental magnesium/phosphorus-transporting channels between healthy and preeclamptic pregnancies. Mol Reprod Dev. 2014; 81:851–60. [PubMed: 25155868]
11. Festing M, Speer M, Yang H, Giachelli C. Generation of mouse conditional null alleles of the type III sodium-dependent phosphate cotransporter PiT-1. Genesis. 2009; 47:858–63. [PubMed: 19882669]

12. Beck L, Leroy C, Beck-Cormier S, Forand A, Salaün C, Paris N, et al. The phosphate transporter PiT1 (Slc20a1) revealed as a new essential gene for mouse liver development. PLoS ONE. 2010; 5:e9148. [PubMed: 20161774]
13. Wallingford MC, Giachelli CM. Loss of PiT-1 results in abnormal endocytosis in the yolk sac visceral endoderm. Mech Dev. 2014; 133:189–202. [PubMed: 25138534]
14. Roberts JM, August PA, Bakris G, Barton JR, Bernstein IM, Druzin M, et al. Hypertension in pregnancy. American College of Obstetricians and Gynecologists. 2013
15. Rhee S, Guerrero-Zayas MI, Wallingford MC, Ortiz-Pineda P, Mager J, Tremblay KD. Visceral endoderm expression of Yin-Yang1 (YY1) is required for VEGFA maintenance and yolk sac development. PLOS ONE. 2013; 8:e58828. [PubMed: 23554936]
16. Trask, M.; Tremblay, KD.; Mager, J. Yin-Yang1 is required for epithelial-to-mesenchymal transition and regulation of Nodal signaling during mammalian gastrulation. Dev Biol. 2012. http://dx.doi.org/10.1016/j.ydbio.2012.05.031
17. Rossant J, Cross JC. Placental development: lessons from mouse mutants. Nat Rev Genet. 2001; 2:538–48. [PubMed: 11433360]
18. Jensen N, Schrøder HD, Hejbøl EK, Füchtbauer EM, de Oliveira JR, Pedersen L. Loss of function of Slc20a2 associated with familial idiopathic Basal Ganglia calcification in humans causes brain calcifications in mice. J Mol Neurosci. 2013; 51:994–9. [PubMed: 23934451]
19. Legati A, Giovannini D, Nicolas G. Mutations in XPR1 cause primary familial brain calcification associated with altered phosphate export. Nat Genet. 2015; 47:579–81. [PubMed: 25938945]
20. Akirav C, Lu Y, Mu J, Qu DW, Zhou YQ, Slevin J, et al. Ultrasonic detection and developmental changes in calcification of the placenta during normal pregnancy in mice. Placenta. 2005; 26:129–37. [PubMed: 15708114]
21. Yurchenco PD, Amenta PS, Patton BL. Basement membrane assembly, stability and activities observed through a developmental lens. Matrix Biol. 2004; 22:521–38. [PubMed: 14996432]
22. Sasaki T, Fässler R, Hohenester E. Laminin: the crux of basement membrane assembly. J Cell Biol. 2004; 164:959–63. [PubMed: 15037599]
23. Wallingford MC, Angelo JR, Mager J. Morphogenetic analysis of peri-implantation development. Dev Dyn. 2013; 242:1110–20. [PubMed: 23728800]
24. Oyane A, Uchida M, Onuma K, Ito A. Spontaneous growth of a laminin-apatite nano-composite in a metastable calcium phosphate solution. Biomaterials. 2006; 27:167–75. [PubMed: 16024072]
25. Bougas K, Stenport VF, Tengvall P, Currie F, Wennerberg A. Laminin coating promotes calcium phosphate precipitation on titanium discs in vitro. J Oral Maxillofac Res. 2011; 2:1–10.
26. Armulik A, Genové G, Mäe M, Nisancioglu MH, Wallgard E, Niaudet C, et al. Pericytes regulate the blood–brain barrier. Nature. 2010; 468:557–61. [PubMed: 20944627]
27. Allegra A, Altomare R, Curcio P, Santoro A, Lo Monte AI, Mazzola S, et al. Gene expression of stem cells at different stages of ontological human development. Eur J Obstet Gynecol Reprod Biol. 2013; 170:381–6. [PubMed: 23932306]
28. Ghosh M, Gerber C, Rahman MM, Vernier KM, Pereira FE, Subramani J, et al. Molecular mechanisms regulating CD13-mediated adhesion. Immunology. 2014; 142:636–47. [PubMed: 24627994]
29. Licona-Limón I, Garay-Canales CA, Muñoz-Paleta O, Ortega E. CD13 mediates phagocytosis in human monocytic cells. J Leukoc Biol. 2015; 98:85–98. [PubMed: 25934926]
30. Edwards JP, Zhang X, Frauwirth KA, Mosser DM. Biochemical and functional characterization of three activated macrophage populations. J Leukoc Biol. 2006; 80:1298–307. [PubMed: 16905575]
31. Mulder R, Banete A, Basta S. Spleen-derived macrophages are readily polarized into classically activated (M1) or alternatively activated (M2) states. Immunobiology. 2014; 219:737–45. [PubMed: 24954891]
32. Emmrich P. Pathology of the placenta. X. Syncytial proliferation, calcification, cysts, pigments and metabolic disorders. Zentralbl Pathol. 1992; 138:77–84. [PubMed: 1610768]
33. Chen K, Chen L, Lee Y. Exploring the relationship between preterm placental calcification and adverse maternal and fetal outcome. Ultrasound Obstet Gynecol. 2011; 37:328–34. [PubMed: 20586039]

34. Bailão LA, Osborne NG, Rizzi MC, Bonilla-Musoles F, Duarte G, Bailão TC, et al. Ultrasound markers of fetal infection Part 1: Viral infections. Ultrasound Q. 2005; 21:295–308. [PubMed: 16344748]
35. Crouthamel MH, Lau WL, Leaf EM, Chavkin NW, Wallingford MC, Peterson DF, et al. Sodium-dependent phosphate cotransporters and phosphate-induced calcification of vascular smooth muscle cells: redundant roles for PiT-1 and PiT-2. Arterioscler Thromb Vasc Biol. 2013; 33:2625–32. [PubMed: 23968976]
36. Chavkin NW, Chia JJ, Crouthamel MH, Giachelli CM. Phosphate uptake-independent signaling functions of the type III sodium-dependent phosphate transporter, PiT-1, in vascular smooth muscle cells. Exp Cell Res. 2015; 333:39–48. [PubMed: 25684711]
37. Sodhi S, Mohan H, Jaiswal T, Mohan P, Rathee S. Placental pathology in pre-eclampsia eclampsia syndrome. Indian J Pathol Microbiol. 1990; 33:11–6. [PubMed: 2394469]
38. Salgado SS, Salgado MKR. Structural changes in pre-eclamptic and eclamptic placentas-an ultrastructural study. J Coll Physicians Surg Pak. 2011; 21:482–6. [PubMed: 21798135]
39. Jiang R, Teng Y, Huang Y, Gu J, Ma L, Li M, et al. Preeclampsia serum-induced collagen I expression and intracellular calcium levels in arterial smooth muscle cells are mediated by the PLC-γ1 pathway. Exp Mol Med. 2014; 46:e115. [PubMed: 25257609]
40. Tannetta DS, Dragovic RA, Gardiner C, Redman CW, Sargent IL. Characterisation of syncytiotrophoblast vesicles in normal pregnancy and pre-eclampsia: expression of Flt-1 and endoglin. PLOS ONE. 2013; 8
41. Yang Y, Liu X, Jia J, Bai Y, Dai L, Wang T, et al. Role of osteoprotegerin gene variants in early-onset severe pre-eclampsia. J Obs Gynaecol Res. 2015; 41:334–42.
42. Lenhart PM, Nguyen T, Wise A, Caron KM, Herring AH, Stuebe AM, et al. Adrenomedullin signaling pathway polymorphisms and adverse pregnancy outcomes. Am J Perinatol. 2014; 31:327–34. [PubMed: 23797962]
43. Lenhart PM, Caron KM. Adrenomedullin and pregnancy: perspectives from animal models to humans. Trends Endocrinol Metab. 2012; 23:524–32. [PubMed: 22425034]
44. Thyboll J, Kortesmaa J, Cao R, Soininen R, Wang L, Iivanainen A, et al. Deletion of the laminin alpha4 chain leads to impaired microvessel maturation. Mol Cell Biol. 2002; 22:1194–202. [PubMed: 11809810]
45. Zhou Z, Doi M, Wang J, Cao R, Liu B, Chan KM, et al. Deletion of laminin-8 results in increased tumor neovascularization and metastasis in mice advances in brief. Cancer Res. 2004; 4:4059–63. [PubMed: 15205311]
46. Miner JH, Cunningham J, Sanes JR. Roles for laminin in embryogenesis: exencephaly, syndactyly, and placentopathy in mice lacking the laminin alpha5 chain. J Cell Biol. 1998; 143:1713–23. [PubMed: 9852162]
47. Hallmann R, Horn N, Selg M, Wendler O, Pausch F, Sorokin LM. Expression and function of laminins in the embryonic and mature vasculature. Physiol Rev. 2005; 85:979–1000. [PubMed: 15987800]
48. Furuhashi N, Kimura H, Nagae H, Yajima A, Kimura C, Saito T. Serum collagen IV and laminin levels in preeclampsia. Gynecol Obs Investig. 1994; 37:250–3.
49. Foidart JM, Hunt J, Lapiere CM, Nusgens B, De Rycker C, Bruwier M, et al. Antibodies to laminin in preeclampsia. Kindey Int. 1986; 29:1050–7.
50. Kurdoglu M, Kurdoglu Z, Ozen S, Kucukaydin Z, Bulut G, Erten R, et al. Expression of laminin receptor 1 in human placentas from normal and preeclamptic pregnancies and its relationship with the severity of preeclampsia. J Perinat Med. 2011; 39:411–6. [PubMed: 21391874]
51. Chung AE, Dong LJ, Wu C, Durkin ME. Biological functions of entactin. Kidney Int. 1993; 43:13–9. [PubMed: 8433553]
52. Boll W, Partin JS, Katz AI, Caplan MJ, Jamieson JD. Distinct pathways for basolateral targeting of membrane and secretory proteins in polarized epithelial cells. Proc Natl Acad Sci U S A. 1991; 88:8592–6. [PubMed: 1656451]
53. Vila-Porcile E, Picart R, Tixier-Vidal A, Tougard C. Cellular and subcellular distribution of laminin in adult rat anterior pituitary. J Histochem Cytochem. 1987; 35:287–99. [PubMed: 3029213]

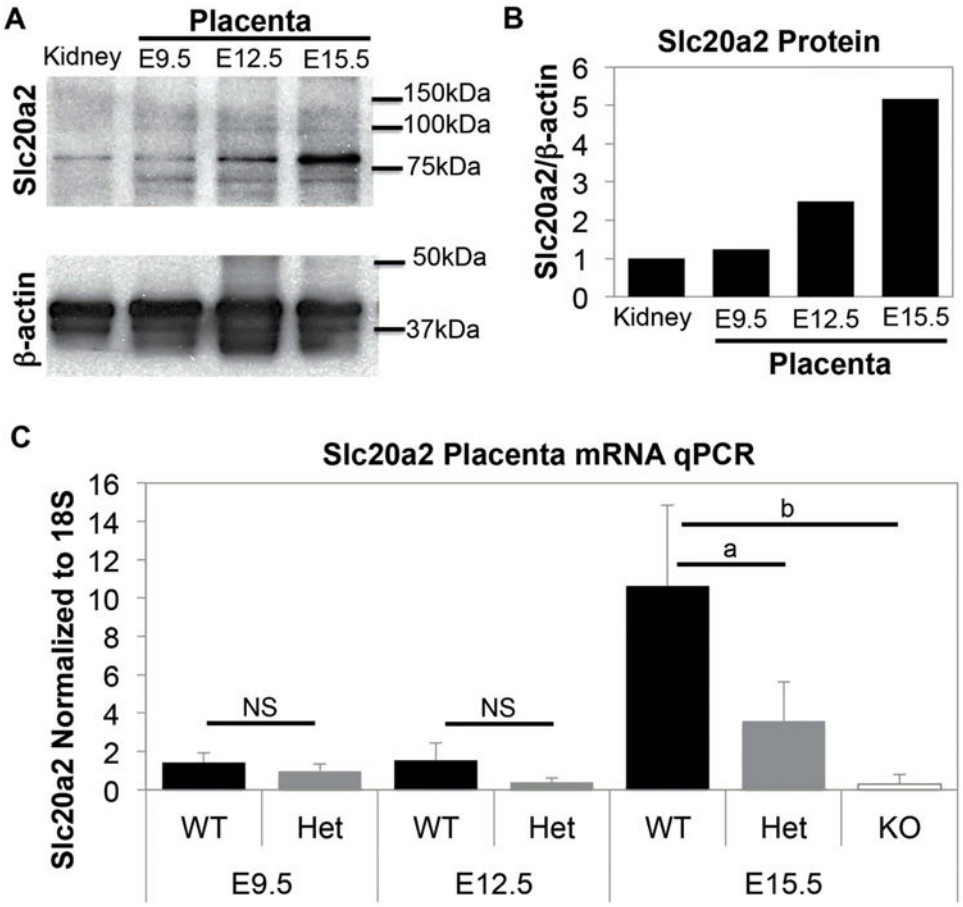

Fig. 1.

Slc20a2 is expressed in mouse placenta. (A) Slc20a2 protein was detected in embryonic day (E) 9.5, E12.5, and E15.5 placental lysates by western blotting. Mouse kidney lysate was used as a positive control. (B) Slc20a2 levels were normalized to β-actin to visualize relative Slc20a2 protein levels. (C) Slc20a2 mRNA qPCR normalized to 18S revealed an increase in Slc20a2 mRNA level during at E15.5. At E15.5, Slc20a2 mRNA is significantly decreased in Slc20a2+/− placenta ($p = 0.031$) and Slc20a2−/− placenta ($p = 0.004$) compared to Slc20a2+/+ placenta. NS: not significant; $^{a}p < 0.05$; $^{b}p < 0.005$.

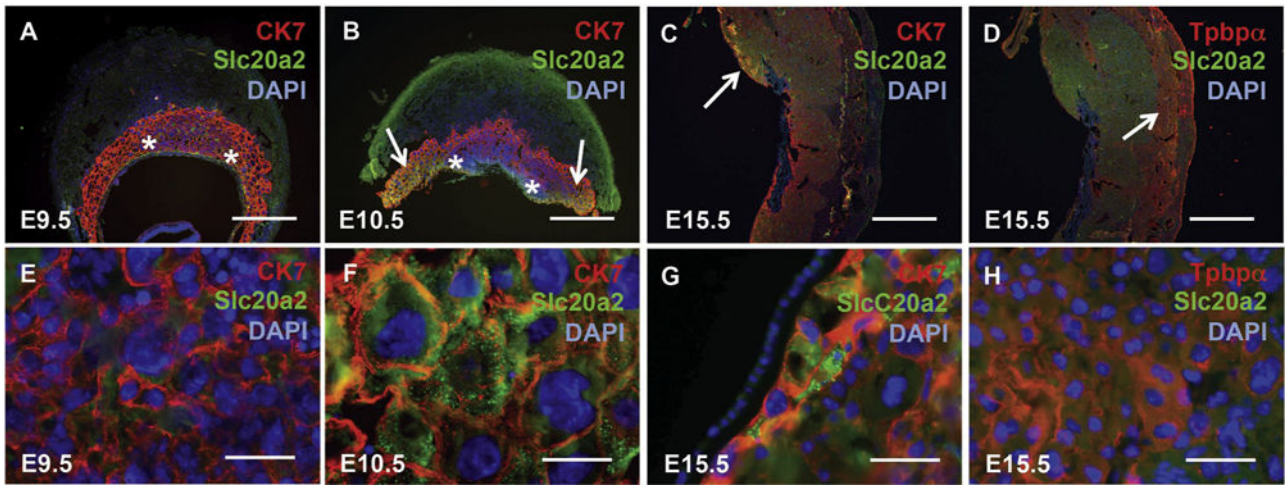

Fig. 2.

Slc20a2 localizes to specific trophoblast cells in the mouse placenta during development. Wildtype embryonic day (E) 9.5, E12.5, E15.5 placental tissue was stained with anti-Slc20a2 antibody and either cytokeratin 7 (CK7) (A–C, E–G) or trophoblast specific protein alpha (Tpbpα) (D, H), and counterstained with DAPI nuclear counterstain. (A–B, E–F) CK7 and Slc20a2 co-localized in a subset of CK7 positive trophoblast cells with large nuclei near the chorioallantoic plate (arrows) that resided just outside of the yolk sac attachment sites (asterisks). E–H are higher magnification views of A–D as follows. E is an image of the labyrinth zone, F and G are images of the chorioallantoic plate outside of the yolk sac attachment sites (arrows in B, C), and H is an image of the spongiotrophoblast layer (arrow in D). Scale bars: A–D = 1 mm, E–H 25 μm.

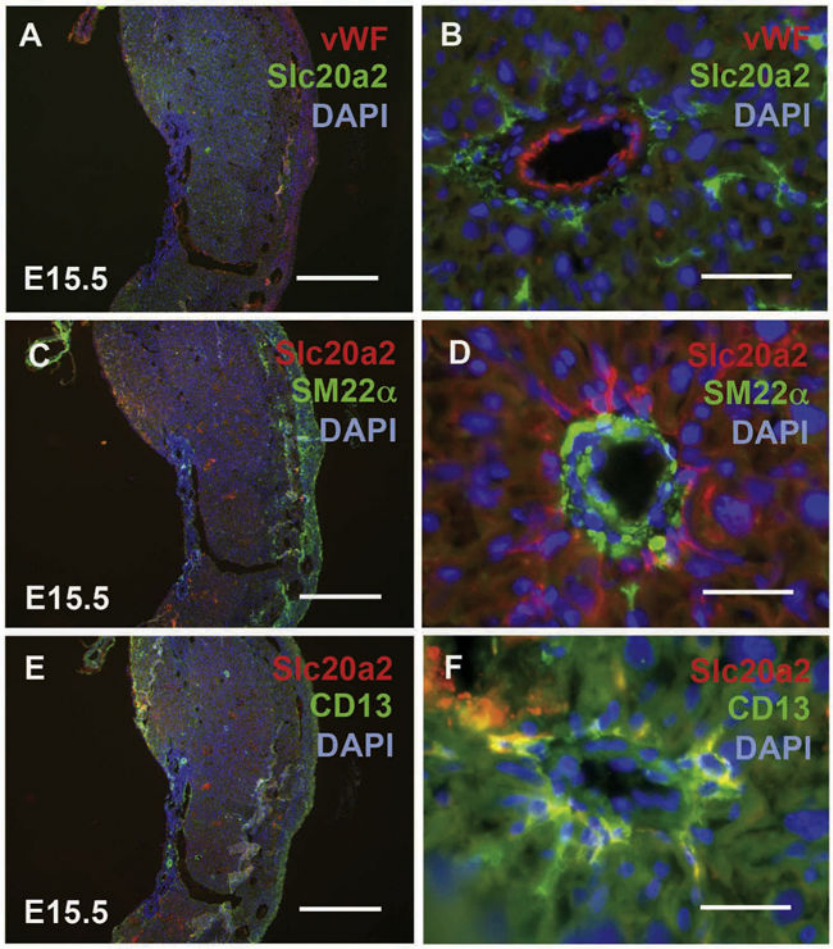

Fig. 3.

Slc20a2 localizes to pericytes in the E15.5 mouse decidua. Wildtype E15.5 placental tissue was stained with anti-Slc20a2 antibody and either von Willebrand factor (vWF) (A, B), smooth muscle 22 alpha (SM22α) (C, D), or aminopeptidase N (CD13) (E, F) and counterstained with DAPI nuclear counterstain. Scale bars: A, C, E = 1 mm; B, D, F = 25 μm.

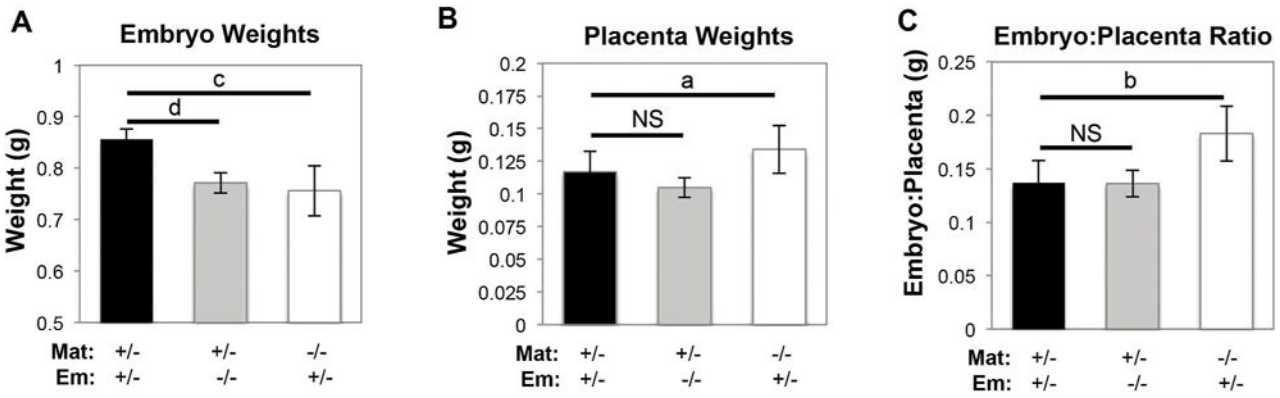

Fig. 4.

Slc20a2 deficiency impacts viability. Complete loss of Slc20a2 from either the embryonic placental compartment (0.0004) or maternal placental compartment ($p = 0.003$) leads to a significant decrease in embryonic weight at E17.5; $N = 14$ with $n = 4–5$ per genotype (A). Complete loss of Slc20a2 from either the embryonic placental compartment ($p = 0.2$) or maternal placental compartment ($p = 0.09$) does not change placental weight significantly at E17.5; $N = 13$ with $n = 4–5$ per genotype (B). Complete loss of Slc20a2 from the embryonic compartment does not change the embryo:placenta ratio ($p = 0.29$), but complete loss from the maternal compartment leads to a significant increase in the embryo:placenta ratio at E17.5 ($p = 0.02$); $n = 4–5$; $N = 13$ (C). NS: not significant; $^{a}p < 0.1$; $^{b}p < 0.05$; $^{c}p < 0.005$; $^{d}p < 0.0005$.

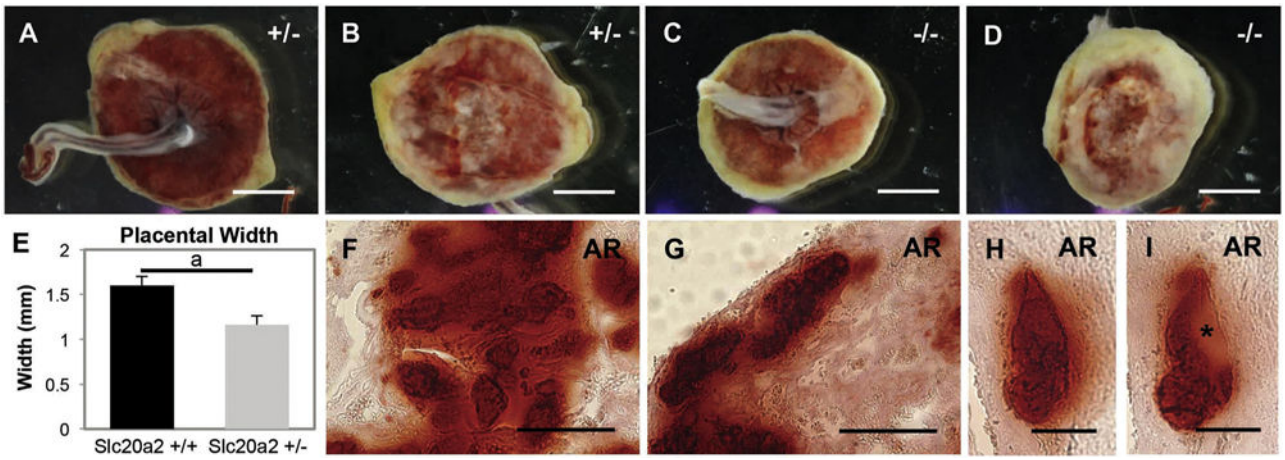

Fig. 5.

Placental calcification is abundant in Slc20a2 deficient placentas. Placentas from Slc20a2+/− females were analyzed. Brightfield whole mount images suggest abnormal vascular development in placentas from Slc20a2−/− embryos compared to those from Slc20a2+/− embryos (A–D). Placentas from Slc20a2+/− females were thinner than control placentas ($p = 0.006$) (E). Positive staining for Alizarin Red was seen in the vascularized labyrinth (F), and the spiral arteries of the decidua (G–I) indicating calcification in these areas. Consecutive sections of calcified spiral arteries revealed nodules of basement membrane-like material highlighted by an asterisk (H, I). Scale bars: A–D = 1 μm, F–G = 50 mm, H–I = 25 μm. $^{a}p < 0.05$.

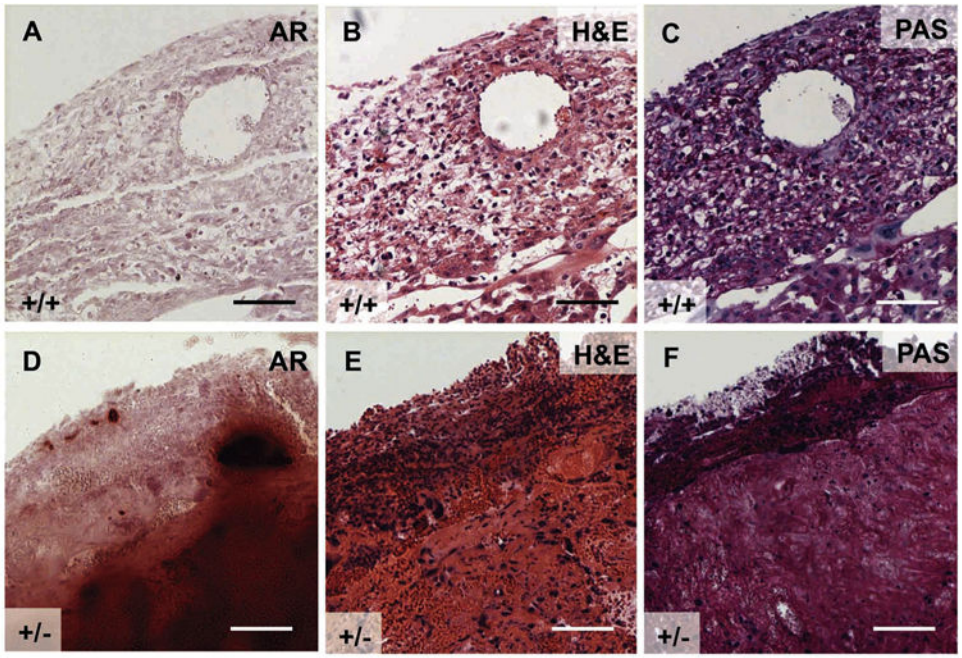

Fig. 6.

Pregnant Slc20a2+/− females with declining health have abnormal decidua. Consecutive E17.5 wildtype and Slc20a2 +/− placenta sections were stained with Alizarin Red (A, D), H&E (B, E), or PAS (C, F). Scale bars: A–F = 100 μm.

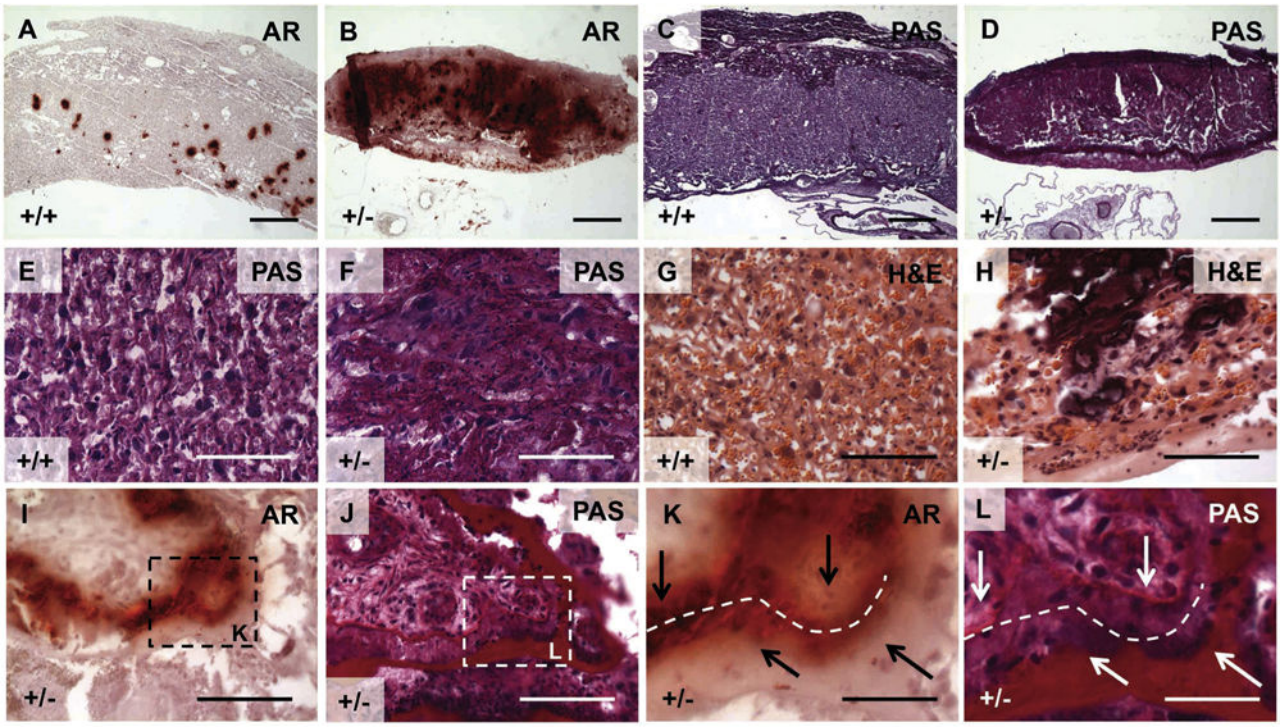

Fig. 7.

Placental histological stains indicate a spatial relationship between placental calcification and basement membrane. We then tested whether placentas from Slc20a2+/+ or Slc20a2+/− females develop distinct placental calcification patterns by staining with Alizarin Red. Alizarin Red staining detected minimal calcification in Slc20a2+/+ placentas compared to Slc20a2 +/− placentas (A, B) and PAS stained adjacent sections revealed abundant deposition of basement membrane (C, D). Similarly, high magnification images of PAS and H&E stained labyrinth tissue revealed abnormal basement membranes in Slc20a2+/− placentas (E–H). Basement membranes encircling the chorioallantoic umbilical cord attachment were frequently lined by calcification, and in some cases, large membranes were split (see arrows in K, L) and the exposed spaced contained Alizarin Red positive mineral (see dashed line in K, L). Scale bars: A–D = 500 mm, E–L = 100 μm.

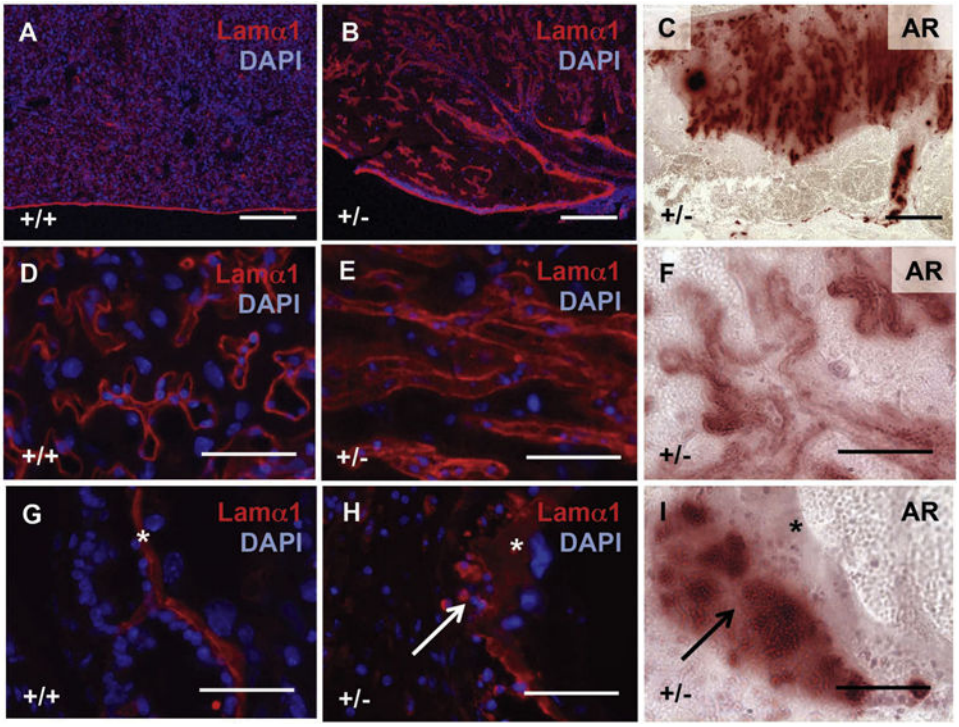

Fig. 8.

Abnormal vasculature associates with placental calcification in Slc20a2 deficient placentas. Detection of Lamα1 with DAPI nuclear counterstaining reveals abnormal vascular structure to the labyrinth (A, B and D, E), as well as thickening of the chorioallantoic plate (G, H). Alizarin Red staining of consecutive sections reveals close proximity of calcified sites to Lamα1 in Slc20a2+/− placentas. Scale bars: A–C = 300 μm, D–I = 50um. Asterisks: basement membrane. Arrows: calcified sites.

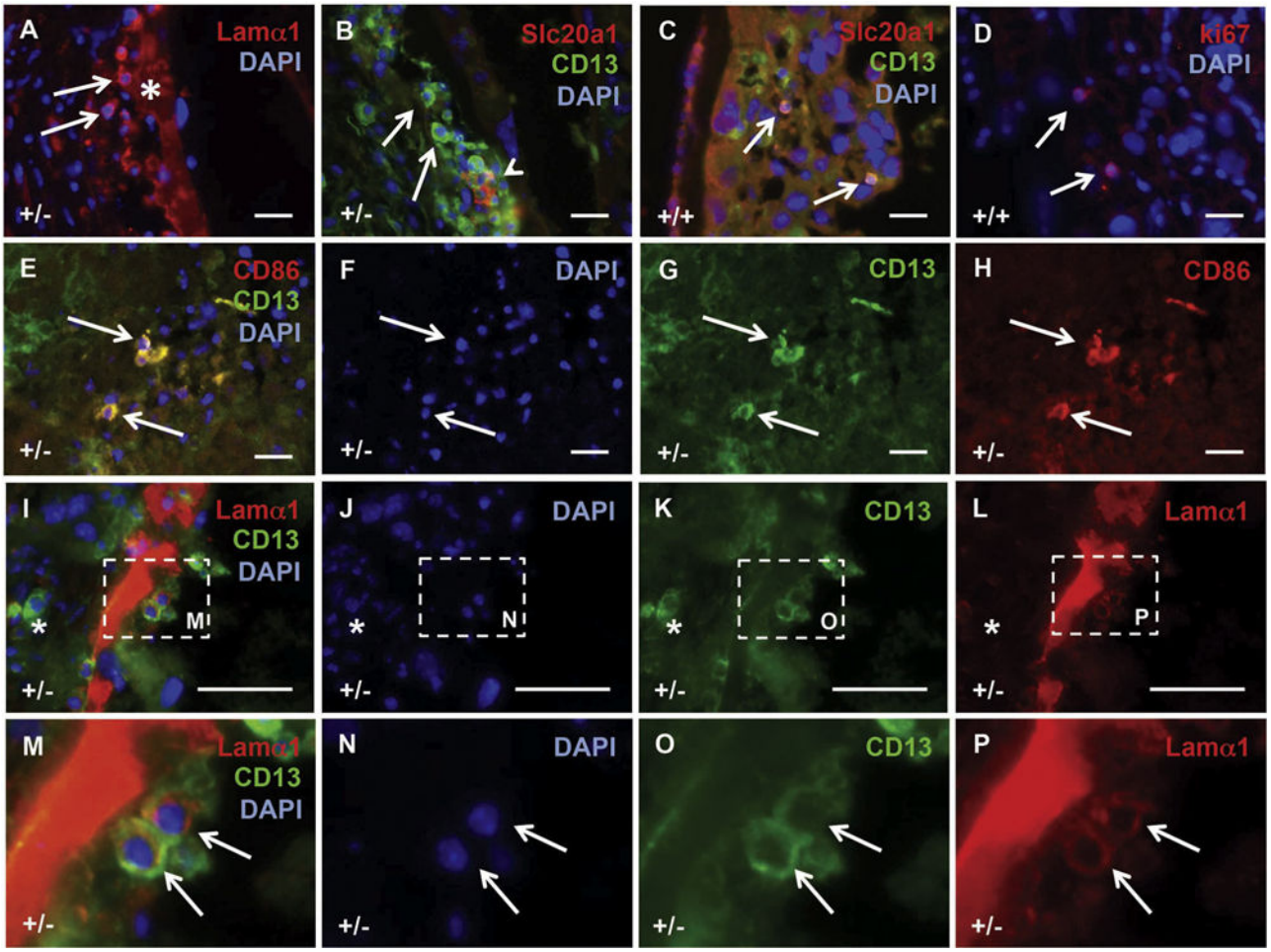

Fig. 9.

A novel Lamα1 and CD13 positive placental cell is present at the calcified sites. Mouse placental tissue from Slc20a2 +/− and Slc20a2+/+ females was stained with a variety of antibodies to characterize the cellular milieu at calcified sites, and to determine the cellular identity of candidate causative cell types. Cells expressing Lamα1 (arrow) were identified adjacent to the enlarged basement membranes (asterisk) in calcified lesions (A). CD13 positive (arrows) and CD13/Slc20a1 positive cells (arrow head) were detected in the calcified lesions (B). Morphologically, similar cells that co-expressed CD13 and Slc20a1 were sparse in WT placenta. Staining of consecutive sections revealed expression of ki67 (D). Round CD13 positive cells in the labyrinth are CD86 positive (E–H). CD13 positive cells at the calcified site adjacent to enlarged basement membranes contain Lamα1 (arrows), while other CD13 positive cells do not (asterisk) (I–P). Scale bars: A–L = 20 μm. M–P: magnified images as indicated by dashed lines in I–L.

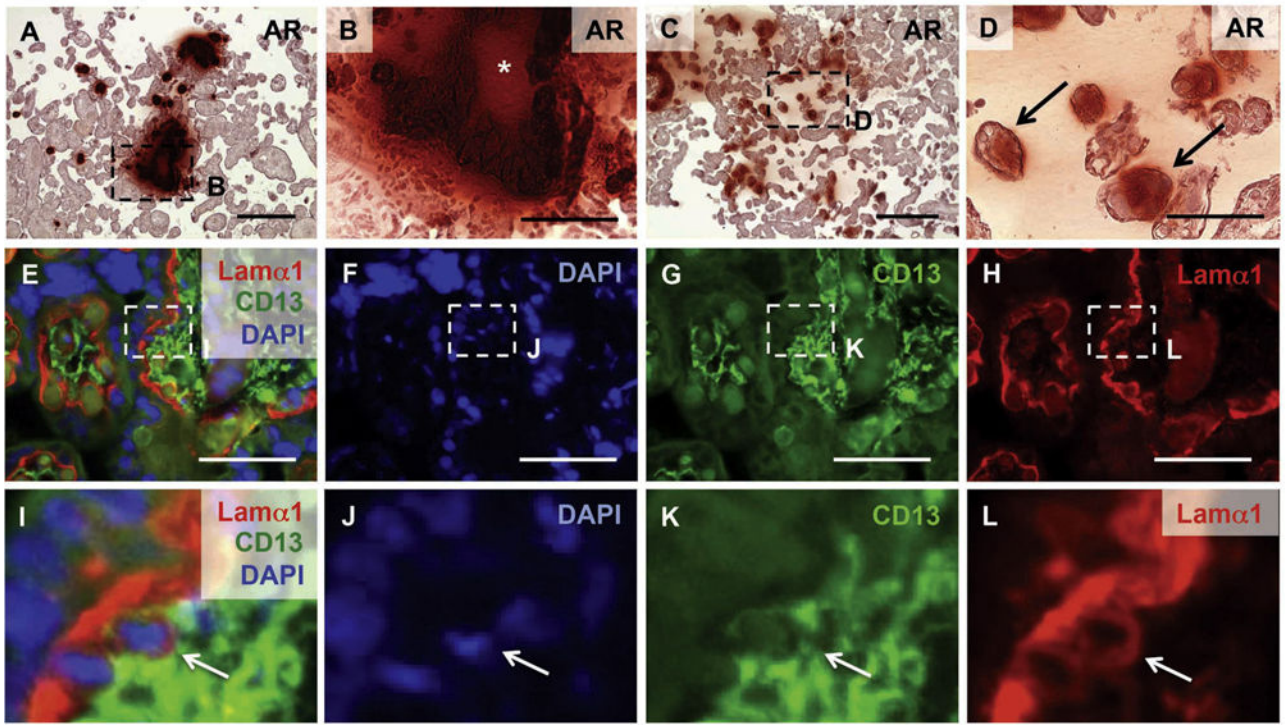

Fig. 10.

Calcified preeclampsia placentas contain a similar Lamα1 positive cell. (A–D) Alizarin Red staining reveals calcification in human placenta ($n = 3$). Some calcified sites contained nodules of basement membrane-like material indicated by an asterisk (B). Arrows indicate calcified tissue in terminal villi (D). Detection of Lamα1 and CD13 with DAPI nuclear counterstain identified comparable Lamα1 positive cells in human placenta (E–L). Scale bars: A, C = 300 μm; B, D = 100 μm; E–H = 20 μm. I–L: magnified images as indicated by dashed lines in E–H.

Table 1

Animals generated by Slc20a2 heterozygous intercrosses.

Parameter	Slc20a2+/+	Slc20a2+/−	Slc20a2−/−	Total
Expected (%)	25	50	25	100
Expected number of animals	42	84	42	168
Experimental (%)	37	49	14	100
Experimental number of animals	42	55	16	113
Lost prior to weaning (%)	0	35	62	N/A

Table 2

Animals generated by Slc20a2 homozygous null intercrosses.

Parameter	Value
Predicted average litter size (het crosses)	9.3
Experimental average litter size	5.5
Experimental number of animals	33
Lost prior to weaning (%)	55